Adaptive Current Controller Based on Neural Network and Double Phase Compensator for a Stepper Motor

Hoang Ngoc Tran, Kien Minh Le, and Jae Wook Jeon, *Member, IEEE*

***Abstract*—In this paper, we propose an advanced approach to improve the accuracy of stepper motors based on an effective phase compensator. The proposed approach includes an adaptive current controller and an adaptive position controller. The proposed adaptive feed-forward proportional-resonant (AFPR) current control technique with a neural network (NN) is an improvement over the conventional proportional-integral algorithm. In which, the NN algorithm is applied to obtain the optimal parameters for the AFPR controller. This results in an enhancement of the stepper motor current tracking. In addition, the advanced position controller is a combination of a damping and a phase-compensated (D&PC) method to reduce steady-state error and variations during low-speed operation. The position tracking performance is further appreciated by applying an advanced proportional integral derivative (PID) controller during high-speed operation. A bandpass filter is designed to switch the motor between low- and high-speed operational regimes. The proposed approach does not require any changes in the structure of the hardware. Therefore, it can be widely applied to a diverse set of industrial applications. The performance of the proposed approach was validated by conducting experiments under practical conditions.**

***Index Terms*—Damping, micro-stepping, neural network (NN), proportional plus resonant (PR) compensator, phase compensation, stepper motor.**

I. Introduction

HYBRID stepper motors have been used in motion control systems because of their low manufacturing cost, reliable structure and simplicity of control. For this reason, investigating advanced control approaches to improve the performance of the stepper motor is an important goal in commercial and industrial applications. One of the main tasks of controlling stepper motors is to achieve the minimum position tracking error over the full speed range. In addition, the use of current tracking control also plays an important role in reducing the position error.

Manuscript received September 3, 2018; accepted October 17, 2018. Date of publication October 30, 2018; date of current version May 22, 2019. This work was supported in part by the MSIP, South Korea, under the G-ITRC Support Program (IITP-2018-20150-00742) supervised by the IITP and in part by the Basic Science Research Program through NRF of South Korea funded by MOE under Grant NRF-2010-0020210. Recommended for publication by Associate Editor A. Muetze. *(Corresponding author: Jae Wook Jeon.)*

The authors are with the School of Information and Communication Engineering, Sungkyunkwan University, Suwon 440-746, South Korea (e-mail:

performance of stepper motor drives. Nonlinear torque control using position and current feedback was applied in [11]. Additionally, many damping algorithms have been employed to reduce vibrations, including the Kalman filter, Jacobian linearization observer, and harmonic injection schemes [12] and [13]. Although these methods demonstrated smooth speeds and good position tracking abilities, these nonlinear control algorithms cannot operate perfectly over the full speed range and require complex calculations. In this paper, we designed a new position controller, which uses a combination of the damping method based on electromagnetic torque modulation and a phase-compensated method to reduce the vibrations and SSPE.

The main contributions of this paper are summarized as follows.

1) An AFPR-NN was designed as an improved current control scheme based on an adaptive PR technique and an NN algorithm to minimize the current error and autocalibration parameters for the current controller. Experimental results showed that the performance of this scheme is much better than PI-based algorithms.
2) An advanced position tracking control method was proposed to guarantee smoothness in speed and minimize the position errors of the stepper motor over the full operating speed range. A low-speed compensator employing a damping and a phase-compensated (D&PC) method and a high-speed compensator with an advanced proportional integral derivative (PID) method was included.
3) All the proposed algorithms were implemented on an industrial digital signal processor (DSP)-based stepping motor drive, and they can be simply applied without incurring additional costs.

The structure of this paper is organized as follows. The mathematical model of the stepper motor is presented in Section II. In Section III, the conventional method and an AFPR-NN method for the current controller are designed, analyzed, and compared. The adaptive position tracking controller using D&PC and an advanced PID algorithm are developed in Section IV. The implementation of the proposed approach and the experimental results are presented in Section V. Finally, the conclusions are given in Section VI.

II. Mathematical Model of the Stepper Motor

The dynamic model of the stepper motor can be represented in the state-space domain, as follows

$$J\frac{d\omega}{dt} = T_E - B\omega - T_d \tag{1}$$

$$J\frac{d\omega}{dt} = -K_t i_a \sin(\theta) + K_t i_b \cos(\theta) - B\omega - T_d \tag{2}$$

where $N\omega = \frac{d\theta}{dt}$ is the mechanical speed of the rotor shaft [rad/s], θ is the electrical position of the rotor [rad], J is the moment of inertial of the motor [kg·m^2], B is the viscous friction coefficient [N·m·s/rad], T_d is the load torque [N·m], and T_E the electromagnetic motor torque [N·m].

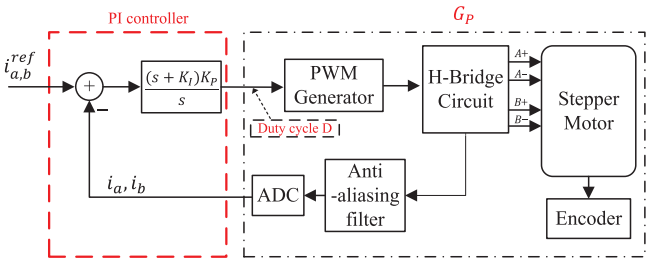

Fig. 1. Block diagram of the current control loop using the conventional PI algorithm.

The electrical equation of the bipolar hybrid stepper motor is considered as [14]

$$L\frac{di_{a,b}}{dt} = v_{a,b} - Ri_{a,b} + e_{a,b} \tag{3}$$

where i_a, i_b and v_a, v_b are the currents and voltages, with corresponding phases of A and B, R is the resistance, L is the inductance of the phase winding, K_t is the motor torque constant, and $e_a = K_t\omega\sin(\theta)$, $e_b = K_t\omega\sin(\theta - \frac{\pi}{2}) = -K_t\omega\cos(\theta)$ are the back-EMF term of each phase. Back-EMF can be defined as sinusoidal disturbances with time-varying frequency. The back-EMF terms are bounded by assuming a stepper motor without step-out.

The reference currents in the two phases of the stepper motor are defined as

$$i_a^{\text{ref}} = I_{\max}\cos(\theta^{\text{ref}})$$

$$i_b^{\text{ref}} = I_{\max}\sin(\theta^{\text{ref}}) \tag{4}$$

where $I_{\max}$ is the amplitude of the reference currents and θ^{ref} is the reference position. The position error $e_\theta = \theta^{\text{ref}} - \theta$ and the velocity error $e_\omega = \omega^{\text{ref}} - \omega$ are defined with reference velocity ω^{ref}. By using the current feedback loops, we can design an AFPR controller that guarantees that the feedback current tracks the reference current perfectly; this will be presented in Section III.

III. Current Controller Design

A. Conventional PI Current Controller

Generally, the PI algorithm is used to design current controllers for practical applications since it can be simply applied and easily tuned. A block diagram of the PI current control system of the stepper motor is shown in Fig. 1. The transfer function expressing the correlation between the input duty cycle (D) of the switching pulses and the output current feedback of the analog-to-digital converter (ADC) sensor is represented as follows [15]

$$G_P(s) = \frac{(1/R)\,K_{\text{scale}}}{(L/R)\,s + 1} \cdot \frac{1}{T_{\text{ali-Filter}}s + 1} \cdot K_{\text{ADC}} \tag{5}$$

where s is the Laplace operator and $T_{\text{ali-Filter}} = 2\pi F_{\text{ali-Filter}}$.

The coefficients of the PI controller were determined by using a zero-cancellation technique and comparing the closed-loop characteristic polynomial of the current control loop to the standard third-order system with the overshoot of 20% and a settling

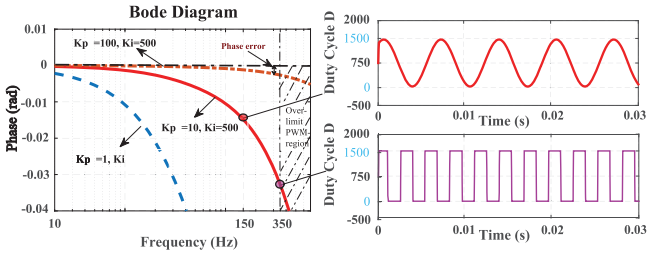

Fig. 2. Bode plot of the PI method and the observation duty cycle value at the boundary.

time 0.0425 ms. The transfer function PI with the chosen parameters (i.e., $K_P \approx 10, K_I \approx 500$) is expressed as

$$G_{\mathrm{PI}}(s) = K_P \frac{(s + K_I)}{s}. \tag{6}$$

The phase-error analysis was carried out using the bode diagram since the speed of the motor changes. As shown in Fig. 2, the error-phase region is smaller when the K_P is large. Unfortunately, the too large value of the parameter K_P causes a very large overshoot. Therefore, the parameters of the PI controller cannot be tuned to reduce the error-phase region further. The bandwidth of the PI controller for adjusting the duty cycle D is bounded, $0 \leq D \leq 1500$, which completely depends on the speed of the MCU. Therefore, when the motor operates above 350 Hz, the PI controller cannot adjust the value of D. To overcome that disadvantages, we proposed the AFPR-NN method to further improve the tracking error performance of the current controller.

B. AFPR-NN Current Controller

1) AFPR Controller Design and Stability Analysis: The proposed AFPR current controller is improved based on the PR technique [16]. It can remove the harmonic at the resonant frequency, but still ensure the stability of the system. We set the resonant frequency (ω_{R_i}) as the frequency of the reference current (or the speed of the rotor shaft ω^{ref}) to achieve the zero error for the current controller. The PR controller can be derived using the transfer function as

$$G_{\mathrm{PR}} = P_{\mathrm{PR}_i} + \frac{K_{R_i}\omega_{R_i} s}{s^2 + (\omega_{R_i}/Q_{R_i})s + \omega_{R_i}^2}. \tag{7}$$

Here, P_{PR_i} is the proportional gain, K_{R_i} is the gain of the resonant terms, and ω_{R_i} is the resonant frequency. The quality factor Q_{R_i} is used [17] to tune the gain of the resonant frequency.

From (7), the dynamic property can be analyzed for simple selection PR parameters based on the bode diagram and root locus method as shown in Fig. 3. The parameter Q_{R_i} is selected to completely remove the phase error at the respective frequency in Fig. 3(a). Meanwhile, the parameter K_{R_i} is selected by the root locus technique. The root locus of the system is farther from the imaginary axis than larger values, so the system will be more stable.

All these constraints are considered, and a comparison between the PI method and PR method at the uniform of step response and frequency response can be seen in Fig. 4. The PR method both satisfied the overshoot and settling time condition

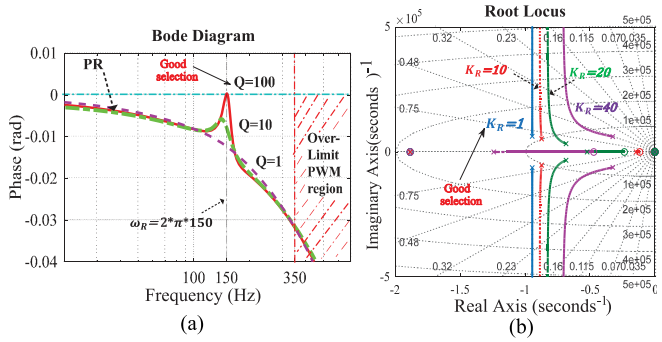

Fig. 3. Selection PR parameters based on the bode plot and the root locus technique when the value of $\omega_{R_{150}}$ at 150 Hz.

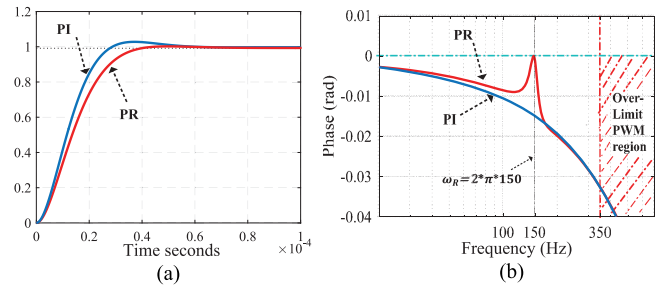

Fig. 4. Comparison between the PI method with $K_P \approx 10, K_I \approx 500$ and PR method with $P_{\mathrm{PR}_{150}} \approx 10, \omega_{R_{150}} = 2\pi 150, K_{R_{150}} \approx 1, Q_{R_{150}} \approx 100$. (a) Step response. (b) Frequency response.

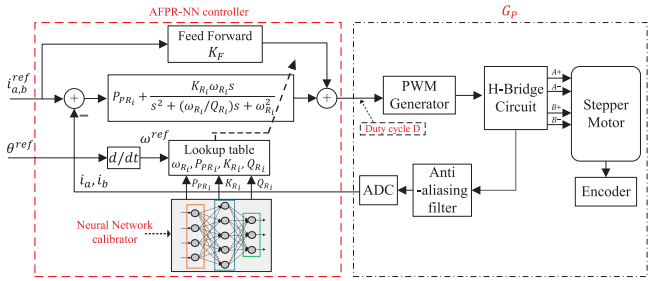

Fig. 5. Block diagram of the current control loop of the proposed AFPR-NN controller.

and completely compensated for the error phase at the resonant frequency.

However, it is impossible to use the PR technique to compensate for the error of the current in the variable frequency domain. Hence, an adaptive current controller was designed (as shown in Fig. 5) by using an offline generated lookup table to store the parameters of the PR controller at each different resonant frequency.

The input of the lookup table is ω^{ref}, and the outputs are P_{PR_i}, K_{R_i}, and Q_{R_i} and $\omega_{R_i} = 2\pi f i$, $\{i = 1 \div 300$ and $f = 1$ Hz$\}$. Furthermore, a feed-forward block is added to the current controller to estimate the total resistance of each phase of the stepper motor. The gain of this block used to enhance the adaptive current resonant controller is calculated as

$$K_F = \frac{1}{n}\sum_{j=1}^{n} \frac{v_{a_j}}{i_{a_j}} \tag{8}$$

where $n = 100$ is the number of initial samples.

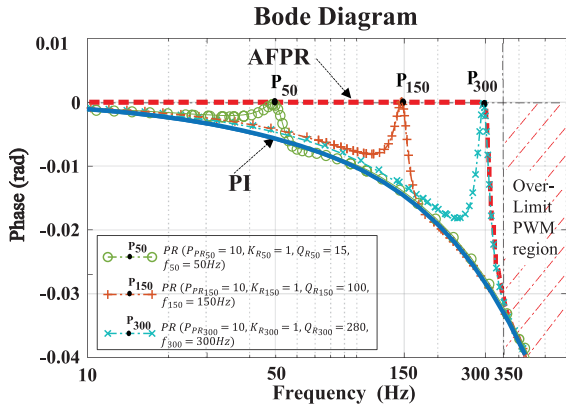

Fig. 6. Bode plot comparison between the PI method and AFPR method.

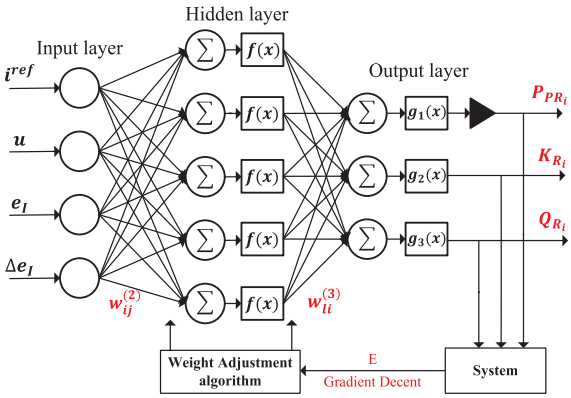

Fig. 7. Three-layer backpropagation network structure.

Finally, the closed-loop transfer function of the AFPR controller and stepper motor from $i_{a,b}^{\text{ref}}$ to $i_{a,b}$ is derived according to Fig. 5 as

$$T_{i_{a,b}^{\text{ref}}\to i_{a,b}}(s)=\frac{[G_{\text{PR}}(s)+K_F]G_P(s)}{1-[G_{\text{PR}}(s)+K_F]G_P(s)}=\frac{K_{\text{PF}_i}s^2+A_1s+K_{\text{PF}_i}\omega_{R_i}^2}{A_2s^4+B_1s^3+B_2s^2+B_3s-K_{\text{PF}_i}\omega_{R_i}^2} \tag{9}$$

where s is the Laplace operator and $K_{\text{PF}_i}=P_{\text{PR}_i}+K_F$, $A_1=K_{\text{PF}_i}\frac{\omega_{R_i}}{Q_{R_i}}+K_{R_i}\omega_{R_i}$, $A_2=\frac{1}{K_{\text{ADC}}}T_{\text{Filter}}L$, $A_3=\frac{1}{K_{\text{ADC}}}T_{\text{Filter}}R$, $B_1=A_2\frac{\omega_{R_i}}{Q_{R_i}}+A_3$, $B_2=A_2\omega_{R_i}^2+A_3\frac{\omega_{R_i}}{Q_{R_i}}-K_{\text{PF}_i}$, and $B_3=A_3\omega_{R_i}^3-A_1$.

The AFPR current controller is capable of improving the performance tracking zero steadystate error with respect to the desired sinusoidal signals at frequencies of 1–300 Hz. Fig. 6 shows the phase responses of the current response at three different frequencies (50, 150, and 300 Hz). We obtained the red dashed line by using 300 samples at 300 frequencies; this is the phase response of the AFPR controller. The phase error appears in PI, but is eliminated by AFPR.

2) Design of the Neural Network to Calibrate the AFPR Controller: However, the dynamic model of the stepper motor with the parameters selected from the bode diagram and root locus method of the AFPR controller does not perfectly reflect the actual motor model, particularly when there is a change of motor. At this point, the parameters of AFPR should be corrected to obtain the smallest error phase. That is why we proposed the NN technique to calibrate the parameters of AFPR by an online backpropagation with the gradient descent update method before storing these parameters in the offline generated lookup table. The parameters will be tuned through the NN training process to obtain the optimal parameters. The incremental digital AFPR control algorithm is expressed as

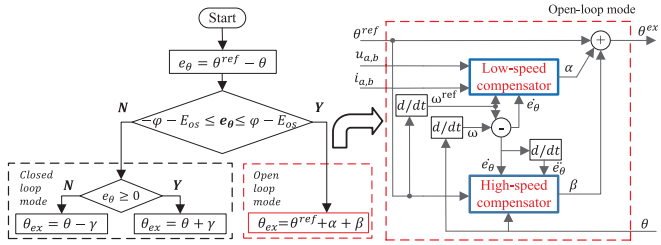

Fig. 8. Loop algorithm and structure of the proposed position control.

$$\begin{aligned}u[k]=&K_{\text{PF}}e_I[k]+(K_{\text{PF}}a_2+a_0)e_I[k-1]\\&+(K_{\text{PF}}a_3+a_1)e_I[k-2]-a_2u[k-1]-a_3u[k-2]\end{aligned} \tag{10}$$

where $u[k]$ is the output of the AFPR controller (D), $e_I[k]=i^{\text{ref}}[k]-i[k]$ is the current error and $a_0=K_{R_i}\omega_{R_i}T_s$, $a_1=-K_{R_i}\omega_{R_i}T_s$, $a_2=\frac{\omega_{R_i}}{Q_{R_i}}T_s-2$, and $a_3=1+\omega_{R_i}^2T_s^2-\frac{\omega_{R_i}}{Q_{R_i}}T_s$.

The NN structure is selected with one hidden layer and five neurons in the hidden layer (see Fig. 7), and the NN outputs are P_{PR_i}, K_{R_i}, Q_{R_i}. The online backpropagation algorithm is applied to tune the weights of the NN to reduce the current tracking error e_I. This backpropagation algorithm is based on the gradient descent update method described in [18].

To achieve the new tuning parameters in the output of the NN, the input for the input layer is given as

$$O_j^{(1)}[k]=x_j[k],(j=1,\dots 4) \tag{11}$$

where $x=[i^{\text{ref}}\ u\ e_I\ \triangle e_I]^T$.

For the hidden layer, the inputs $\left(I_i^{(2)}[k]\right)$ and output $\left(O_i^{(2)}[k]\right)$ are as follows:

$$I_i^{(2)}[k]=\sum_{j=0}^{4}\omega_{ij}^{(2)}O_j^{(1)}[k] \tag{12}$$

$$O_i^{(2)}[k]=f\left(I_i^{(2)}[k]\right),(i=1,\dots 5) \tag{13}$$

where $\omega_{ij}^{(2)}$ are the weights of the hidden layer. The activation function of neurons in the hidden layer is a sigmoid function with positive and negative symmetry $\left(f(x)=\frac{e^x-e^{-x}}{e^x+e^{-x}}\right)$.

The inputs and outputs of the output layer are as follows:

$$I_l^{(3)}[k] = \sum_{i=0}^{5} \omega_{li}^{(3)} O_i^{(2)}[k] \tag{14}$$

$$O_l^{(3)}[k] = g_l\left(I_l^{(3)}[k]\right), (l = 1, 2, 3) \tag{15}$$

where $O^{(3)} = [P_{\mathrm{PR}_i}\ K_{R_i}\ Q_{R_i}]^T$. The activation function of neurons in the output layer should use a nonnegative sigmoid function $\left(g_{1,2}(x) = \frac{e^x}{e^x + e^{-x}}\right)$ and a soft-plus function $(g_3(x) = \log_e(1 + e^x))$.

On the other hand, to update the weights, the quadratic performance index of the current error is proposed as

$$E[k] = \frac{1}{2} e_I^2[k] = \frac{1}{2}(i^{\mathrm{ref}}[k] - i[k])^2 \tag{16}$$

$$\triangle\omega_{li}^{(3)}[k] = -\eta \frac{\partial E[k]}{\partial \omega_{li}^{(3)}[k]} + \upsilon \triangle\omega_{li}^{(3)}[k-1] \tag{17}$$

where η is the learning rate and υ is the inertial term. These coefficients directly affect the evolution and convergence speed of the NN. In order to minimize current error, the $E[k]$ must be tuned to converge to zero in the steady state given by

$$\frac{\partial E[k]}{\partial w_{li}^{(3)}[k]} = \frac{\partial E[k]}{\partial i[k]} \cdot \frac{\partial i[k]}{\partial u[k]} \cdot \frac{\partial u[k]}{\partial O_l^{(3)}[k]} \cdot \frac{\partial O_l^{(3)}[k]}{\partial I_l^{(3)}[k]} \cdot \frac{\partial I_l^{(3)}[k]}{\partial w_{li}^{(3)}[k]} \tag{18}$$

where $\frac{\partial I_l^{(3)}[k]}{\partial \omega_{li}^{(3)}[k]} = O_i^{(2)}[k]$ are the outputs of the hidden layer, $\frac{\partial i[k]}{\partial u[k]}$ is replaced by the sgn $\left(\frac{\partial i[k]}{\partial u[k]}\right)$ approximation, the expressions for $\frac{\partial u[k]}{\partial O_1^{(3)}[k]} = e_I[k] + a_2 e_I[k-1] + a_3 e_I[k-2]$, $\frac{\partial u[k]}{\partial O_2^{(3)}[k]} = \omega_{R_i} T_s (e_I[k-1] - e_I[k-2])$, and $\frac{\partial u[k]}{\partial O_3^{(3)}[k]} = -\frac{a_0 e_I[k-1] + a_1 e_I[k-2] - \omega_{R_i} T_s (u[k-1] + u[k-2])}{Q_{R_i}^2}$.

Thus, the weights of the learning algorithm in output layer can be computed as

$$\triangle\omega_{li}^{(3)}[k] = \upsilon \triangle\omega_{li}^{(3)}[k-1] + \eta \delta_l^{(3)} O_i^{(2)}[k] \tag{19}$$

$$\delta_l^{(3)} = e_I[k] sgn\left(\frac{\partial i[k]}{\partial u[k]}\right) \frac{\partial u[k]}{\partial O_l^{(3)}[k]} \dot{g}_l\left(I_i^{(3)}[k]\right). \tag{20}$$

Using the similar calculation, the weights in hidden layer can be expressed as

$$\triangle\omega_{ij}^{(2)}[k] = \upsilon \triangle\omega_{ij}^{(2)}[k-1] + \eta \delta_i^{(2)} O_j^{(1)}[k] \tag{21}$$

$$\delta_i^{(2)} = \dot{f}\left(I_i^{(2)}[k]\right) \sum_{l=1}^{3} \delta_l^{(3)} \omega_{li}^{(3)}[k], (i = 1, \ldots 5). \tag{22}$$

By using (19) and (21), the weights of NN are updated step by step; the approximating error is reduced accordingly. The learning rate η is selected by error method. If η is small, the time required to make approximating current error approach zero is longer. Moreover, when η is too large, the approximating error fluctuates unstably. Due to the training at different frequencies, η should be a balance between time and stability. Finally, the PR parameters are tuned to obtain the smallest error.

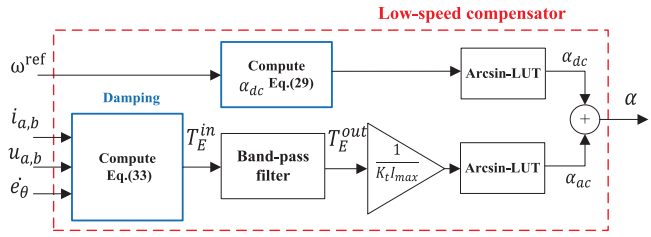

Fig. 9. Block diagram of the low-speed compensator.

IV. Stability Analysis and Design of the Position Controller

The motor position performance is improved due to the effectiveness of the proposed AFPR-NN current controller. However, the SSPE is still large at low frequencies. When the stepper motor operates at high frequencies, the position error vibrates with a large amplitude. To ameliorate this problem, we applied the lead-angle (LA) technique [19] and proposed the D&PC method and an advanced PID method as a compensator controller to enhance the quality of the position control of the motor in an open-loop mode. The compensator includes two parts (i.e., a lowspeed compensator and a high-speed compensator); it can be combined with the LA method in the closed-loop mode to guarantee good performance of the motor at high speed [19]. The algorithm and structure of the proposed compensator are shown in Fig. 8 (γ is the LA value based on the speed, while α, and β are the compensation values of the low-speed and the high-speed compensator, respectively). The definition of the low-speed and high-speed position controller regimes are described as follows.

A. In the Low-Speed Range

The compensation phase α is added to the phase excitation angle (θ_{ex}) to reduce the SSPE and minimize vibration of the transient position error in the low-speed region as shown in Fig. 9. To analyze the proposed algorithm, the position error e_θ will be separated to the steady-state error response $(\triangle\theta_{\mathrm{dc}})$ due to the constant velocity command and the transient response $(\triangle\theta_{\mathrm{ac}})$ to external torque variations. So

$$e_\theta = \theta^{\mathrm{ref}} - \theta = \triangle\theta_{\mathrm{dc}} + \triangle\theta_{\mathrm{ac}}. \tag{23}$$

In addition, $\triangle\theta_{\mathrm{ac}}$ is assumed to be small and $\triangle\theta_{\mathrm{dc}}$ must be smaller than 90° to avoid loss of step given by

$$|\triangle\theta_{\mathrm{ac}}| < 30^\circ \Rightarrow \begin{cases} \cos\triangle\theta_{\mathrm{ac}} \approx 1 \\ \sin\triangle\theta_{\mathrm{ac}} \approx 0 \end{cases} \quad |\triangle\theta_{\mathrm{dc}}| < 90^\circ. \tag{24}$$

In this research, we designed the reference currents for D&PC method (i.e., i_a^{ref} and i_b^{ref}) with compensation phase of α to reduce the steady-state position error and the transient position

TABLE I
EzM-42M-A-J MOTOR PARAMETERS

Parameter	Value
Source Voltage (V_d)	24 V
Current Rate (I)	0.85 A
Phase Resistance (R)	5.45 Ω
Phase Inductance (L)	9.3078 mH
Motor Torque Constant (K_t)	0.83 $N.m/A$
Viscous Friction Coefficient (B)	0.0013 $N.m.s/rad$
Moment of Inertial (J)	5.4×10^{-5} $kg.m^2$
Load torque (T_d)	0.44 $N.m$
Number of Poles (N_r)	50
Cut-Off Frequency of Antialiasing Filter ($F_{ali-Filter}$)	30 kHz
Gain of ADC Sensor (K_{ADC})	$(2^{11}-1)/0.85$
Duty cycle (D)	$(0 \le D \le 1500)$
Convert D from Integer to Time Unit (seconds) (K_{scale})	$(48/1480)$

error in the low-speed region as

$$i_a^{\text{ref}} = I_{\max}\cos(\theta^{\text{ref}} + \alpha)$$
$$i_b^{\text{ref}} = I_{\max}\sin(\theta^{\text{ref}} + \alpha) \tag{25}$$

where $\alpha = \alpha_{\text{dc}} + \alpha_{\text{ac}}$ include the steady-state compensation value α_{dc} and the transient compensation value α_{ac}.

Based on the equation of the motor shaft velocity, we can analyze the effect of the proposed control law by substituting α into (2), with $i_a \equiv i_a^{\text{ref}}$ and $i_b \equiv i_b^{\text{ref}}$, given by

$$J\frac{d\omega}{dt} = K_t I_{\max}\sin\left(\theta^{\text{ref}} - \theta + \alpha\right) - B\omega - T_d. \tag{26}$$

Substituting $e_\theta = \triangle\theta_{\text{dc}} + \triangle\theta_{\text{ac}}$ and $\alpha = \alpha_{\text{dc}} + \alpha_{\text{ac}}$ into (26), we obtain

$$J\frac{d\omega}{dt} = K_t I_{\max}\sin\left(\triangle\theta_{\text{dc}} + \triangle\theta_{\text{ac}} + \alpha_{\text{dc}} + \alpha_{\text{ac}}\right) - B\omega - T_d. \tag{27}$$

Noting that $\triangle\theta_{\text{dc}}$ is constant, it follows that $\triangle\dot{\theta}_{\text{dc}} = 0$. By substituting $N\omega = \frac{d\theta}{dt}$ into (23), the velocity $\omega = \omega^{\text{ref}} - \omega_{\text{ac}}$.

From the definitions in [20] and [21], the value of α_{dc} and α_{ac} can be computed by separating them into steady-state and transient equations.

The steady-state equation to determine α_{dc} is as follows:

$$0 = K_t I_{\max}\sin(\triangle\theta_{\text{dc}} + \alpha_{\text{dc}}) - B\omega^{\text{ref}} - T_{d_{\text{dc}}} \tag{28}$$

$$\alpha_{\text{dc}} = \arcsin\left(\frac{B\omega^{\text{ref}} + T_{d_{\text{dc}}}}{K_t I_{\max}}\right) - \triangle\theta_{\text{dc}} \tag{29}$$

where $\triangle\theta_{\text{dc}}$ is expected to be approximately zero when we add α_{dc} into the phase of reference currents. Therefore, in the low-speed range, $\triangle\theta_{\text{dc}}$ is zero ($\triangle\theta_{\text{dc}} = 0^\circ$) and

$$\max(\alpha_{\text{dc}}) = \max\left\{\arcsin\left(\frac{B\omega^{\text{ref}} + T_{d_{\text{dc}}}}{K_t I_{\max}}\right)\right\} = 90^\circ. \tag{30}$$

The stepper motor has the motor parameters given in Table I. Using this information and (30), $\max(\omega^{\text{ref}}) \approx 543(\text{rad/s}) \approx 86(\text{Hz})$ corresponding to $\max(\alpha_{\text{dc}}) = 90^\circ$. When the motor is operating at a higher frequency, the value of α_{dc} still is 90° to avoid loss of step.

We now arrive at the transient equation to determine α_{ac} given by

$$J\frac{d\omega_{\text{ac}}}{dt} + B\omega_{\text{ac}} + T_{d_{\text{ac}}} = K_t I_{\max}\sin\left(\triangle\theta_{\text{ac}} + \alpha_{\text{ac}}\right). \tag{31}$$

The value of α_{ac} is selected to minimize vibration of the motor, and prevent an unstable situation. In (31), we are interested in the electromagnetic motor torque $T_{E_{\text{ac}}}$, which is generated by the interactions between the permanent magnet rotor field and the stator currents, given by

$$T_{E_{\text{ac}}} = J\frac{d\omega_{\text{ac}}}{dt} + B\omega_{\text{ac}} + T_{d_{\text{ac}}} = K_t I_{\max}\sin\left(\triangle\theta_{\text{ac}} + \alpha_{\text{ac}}\right). \tag{32}$$

Moreover, $T_{E_{\text{ac}}}$ can be written based on the conservation of the capacity formula as

$$T_{E_{\text{ac}}} = \frac{P_{\text{input}} - P_{R_{\text{loss}}} - P_{L_{\text{loss}}}}{\omega^{\text{ref}} - \omega} \tag{33}$$

where $P_{\text{input}} = v_a i_a + v_b i_b$ is the power input of the stepper motor, $P_{R_{\text{loss}}} = R_a i_a^2 + R_b i_b^2$ is the power loss due to the resistance of the coil, and $R_{L_{\text{loss}}} = L\frac{di_a}{dt} i_a + L\frac{di_b}{dt} i_b$ is the power loss caused by the winding when the current changes.

Finally, compensation phase α_{ac} can be easily determined with an expected value of $\triangle\theta_{\text{ac}}$ equal to zero as

$$\alpha_{\text{ac}} = \arcsin\left(\frac{P_{\text{input}} - P_{R_{\text{loss}}} - R_{L_{\text{loss}}}}{K_t I_{\max}(\omega^{\text{ref}} - \omega)}\right). \tag{34}$$

Since the low-speed compensator is used at low frequencies, we designed a bandpass filter to remove noise and limit the value of compensation phase, when the operational frequency exceeded 350 Hz (over the limit of the PWM region). The bandpass filter includes two parts, a high-pass filter (HPF) and a low-pass filter (LPF), and is used to determine the value of $T_{E_{\text{ac}}}$ the computed signal.

First, we use the second-order filter of a Butterworth HPF. The transfer function from $T_{E_{\text{ac}}}^{\text{in}}$ to $T_{E_{\text{ac}}}^{\text{out}}$ is generally defined as

$$\frac{T_{E_{\text{ac}}}^{\text{out}}}{T_{E_{\text{ac}}}^{\text{in}}} = \frac{\omega_{c1}^2 s^2}{s^2 + 2n_1\omega_{c1}s + \omega_{c1}^2} \tag{35}$$

where $\omega_{c1} = 2\pi f_{c1}$ is the cutoff frequency for the HPF ($f_{c1} = 5\,\text{Hz}$) an n_1 is the quality factor. The second-order filter of a Butterworth HPF is used to minimize the transition band for smooth operation of the motor.

Next, the second-order filter of a Butterworth LPF is used to limit the impact of the low-speed compensator below 350 Hz, which is defined as

$$\frac{T_{E_{\text{ac}}}^{\text{out}}}{T_{E_{\text{ac}}}^{\text{in}}} = \frac{\omega_{c2}^2}{s^2 + 2n_2\omega_{c2}s + \omega_{c2}^2} \tag{36}$$

where $\omega_{c2} = 2\pi f_{c2}$ is the cutoff frequency for the LPF ($f_{c2} = 350$ Hz) and n_2 is the quality factor. The quality factor impacts the peakiness of this resonance peak that is its height and narrowness around the cutoff frequency point. Generally to maintain stability, the quality factor $n_1 = n_2 = 1/\sqrt{2}$ should be selected.

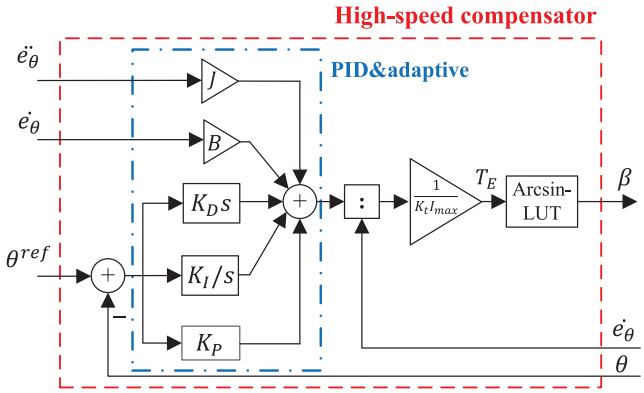

Fig. 10. Block diagram of the high-speed compensator.

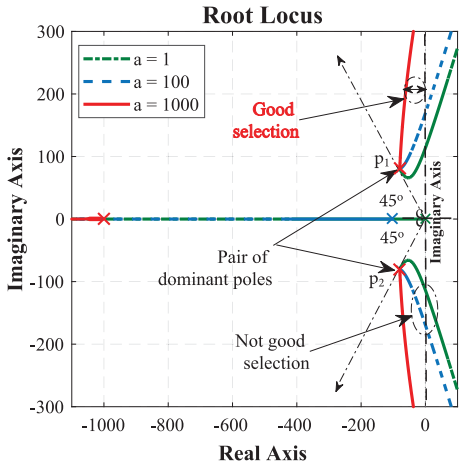

Fig. 11. Root of the characteristic function.

B. In the High-Speed Range

The desirable high-frequency operation of the motor can be achieved in an effectively designed LA controller. However, the vibration and position error of the motor is greater at high speeds over 350 Hz. The controller proposed in low-speed regime depends on the capacity computed from the feedback signal, which is not controllable. Therefore, we propose a method to overcome these problems by considering the compensation phase β to be the same as compensation phase α (see Fig. 10) given by

$$\beta = \arcsin\left(\frac{T_E}{K_t I_{\max}(\omega^{\text{ref}} - \omega)}\right). \tag{37}$$

The electromagnetic torque is not simply computed based on $i_{a,b}$, $u_{a,b}$, and ω feedback, which are considered to be the inputs of the system. The PID controller is used to adjust T_E for tracking the position error. In addition, the error-velocity reference and error-acceleration reference are added to the PID controller to reduce vibrations when the motor operates in high-speed regions given by

$$T_E = K_p\left(\theta^{\text{ref}} - \theta\right) + K_i\int_0^t \left(\theta^{\text{ref}} - \theta\right)dt + K_d\frac{d\left(\theta^{\text{ref}} - \theta\right)}{dt} + B(\omega^{\text{ref}} - \omega) + J\frac{d(\omega^{\text{ref}} - \omega)}{dt}. \tag{38}$$

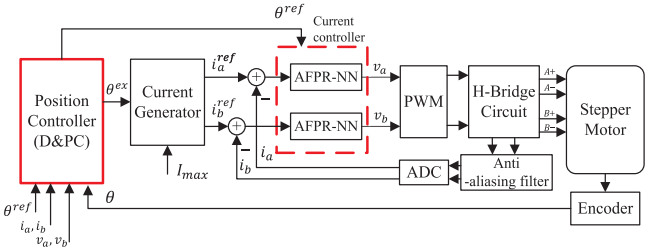

Fig. 12. Block diagram of the proposed controller structure.

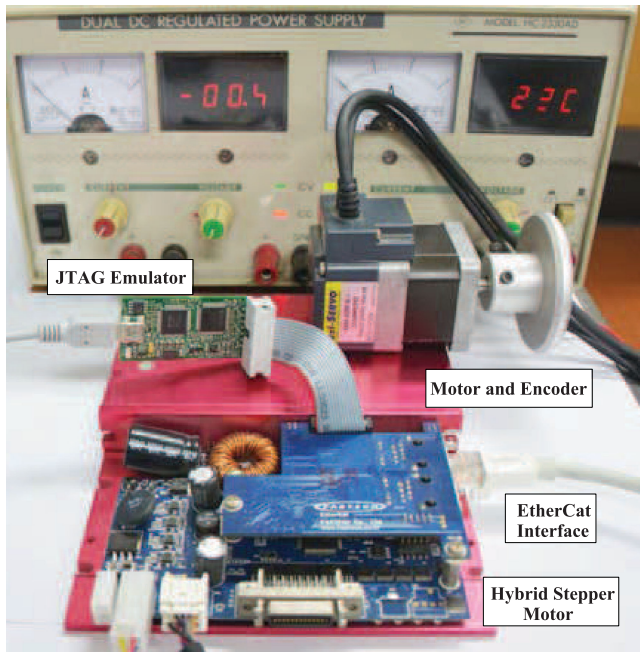

Fig. 13. Experimental system.

Substituting (26) into (42), we obtain

$$e_\theta = \frac{T_E}{Js^3 + (K_d + B)s^2 + K_p s + K_i} \tag{39}$$

where K_p, K_i, and K_d are the coefficients of the PID controller. The characteristic function is

$$s^3 + \frac{(K_d + B)}{J}s^2 + \frac{K_p}{J}s + \frac{K_i}{J} = 0. \tag{40}$$

The behavior of the system is based on the roots of this characteristic function. The root locus of (40) is used in the following analysis to select the proper value of the PID parameters to minimize the position errors and vibrations of the motor. The stable characteristic function with a pair of dominant complex conjugate poles $p_{1,2} = -\xi\omega_n \pm j\omega_n\sqrt{1-\xi^2}$ of the third order system is expressed as

$$s^3 + (a + 2\xi\omega_n)s^2 + (\omega_n^2 + 2a\xi\omega_n)s + a\omega_n^2 = 0 \tag{41}$$

where the natural frequency $\omega_n \approx 114$ and the damping factor $\xi \approx 1/\sqrt{2}$ are assumed. The ω_n should be large so as achieve a fast converging time and the ξ is selected to obtain a small overshoot.

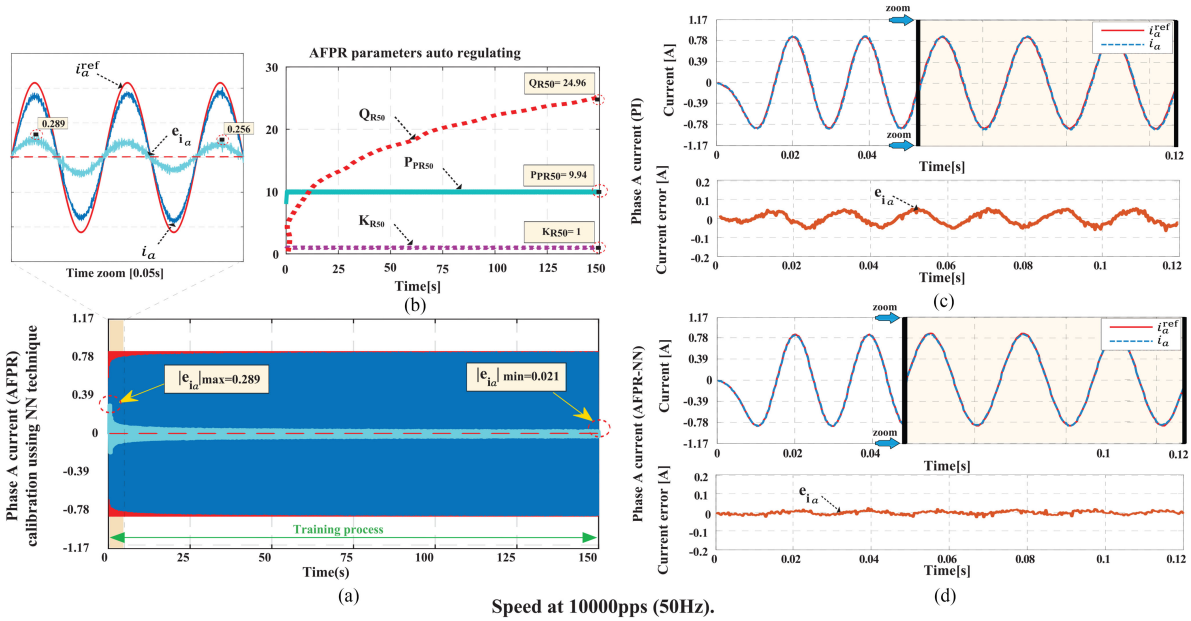

Fig. 14. NN calibration and current tracking performances of the conventional PI controller and the proposed AFPR-NN controller with $P_{\mathrm{PR}} \approx 9.94$, $K_R \approx 1$, $Q_R \approx 24.96$ at 50 Hz.

Balancing the coefficients of (40) and (41) gives

$$\begin{cases} K_d = J(a + 2\xi\omega_n) - B \\ K_p = J(\omega_n^2 + 2a\xi\omega_n) \\ K_i = Ja\omega_n^2. \end{cases} \tag{42}$$

The root of characteristic function (40) is shown in Fig. 11. The value of coefficient a is observed at $1, 100$, and 1000. A good tradeoff between rapidity and stationary can be get when the pair of dominant complex conjugate poles is located around the line of 45° from the negative real axis. The pole is impacted by the coefficient (a), which should be far from the imaginary axis, in order to improve the response rapidity. Moreover, when the value is larger than 1000, the system's stable response is approximate. Therefore, the coefficient (a) is selected to be 1000 and the PID parameters are determined.

V. Experimental Results

A. System Configuration

A block diagram of the proposed controller is shown in Fig. 12 and the experimental system was constructed as shown in Fig. 13. The DSP TMS320F2812 was used to apply the proposed algorithms. The sampling time of our implementation was 25 μs. The controller was coded and commanded by a PC using the JTAG emulator. We used a stepper motor attached to an optical encoder (Fastech, Co., motor model EzM-42M-A-J) with the parameters given in Table I. The current was measured with a 12 bit ADC. The encoder has 10 000 pulses/rev, and was used to evaluate the position tracking performance. The band-pass filter is used with a low cutoff frequency of 5 Hz and a high cutoff frequency of 350 Hz because the proposed position controller was split into two parts (a low-speed compensator and a high-speed compensator).

B. Experimental Results of the Calibration Process and the Current Controller

The calibration process was performed before the official motor activity to select the optimal parameters for the AFPR controller to minimize the current error. The NN training time is set 150 s at each speed in the frequency region from 1 Hz to 300 Hz. In addition, the learning coefficient η and the inertia term ν were assumed to be $\eta = 0.5$ and $\upsilon = 0.24$. Figs. 14(a), 15(a), and 16(a) show that the current error deceases over the training time due to the online backpropagation algorithm. The final parameters of AFPR controller at the lowest current error in Figs. 14(b), 15(b), and 16(b) were stored in the offline generated lookup table.

After the calibration experiment, the results of the current step test and the current sweep test were measured specifically to demonstrate the advanced nature of the proposed methods. In the step test, the current tracking performances of both methods are shown in Figs. 14(a) and (b), 15(a) and (b), and 16(a) and (b). We see that the conventional PI results $(K_P \approx 10, K_I \approx 500)$ in a larger current error, i.e., more than two times the proposed AFPR-NN method. Moreover, we performed the sweep test to test the continuous impact of the AFPR-NN method. The reference velocity and the current error of the sweep test are shown in Fig. 17. The motor runs from 0 and 300 Hz within 1 s, and the current errors of both methods are shown in Fig. 17(b). It is easy to see that the AFPRNN method can minimize the current error better than the PI method. Therefore, we concluded that the proposed method obtains higher accuracy of current tracking performance and better stability. This is a novel improvement that is easy to apply to the current system.

C. Experimental Results of a Low-Speed Compensator

The effectiveness of the APFR-NN controller is demonstrated by the fact that it reduces both the current error and

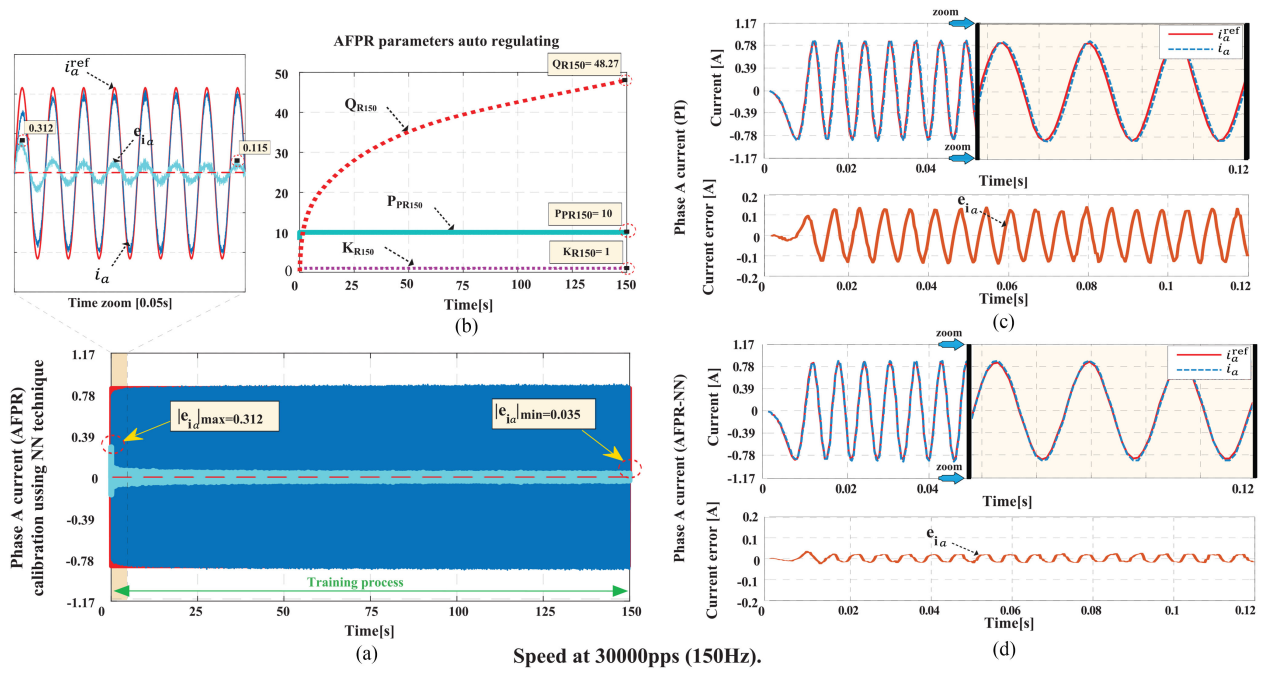

Fig. 15. NN calibration and current tracking performances of the conventional PI controller and the proposed AFPR-NN controller with $P_{\mathrm{PR}} \approx 10$, $K_R \approx 1$, $Q_R \approx 48.27$ at 150 Hz.

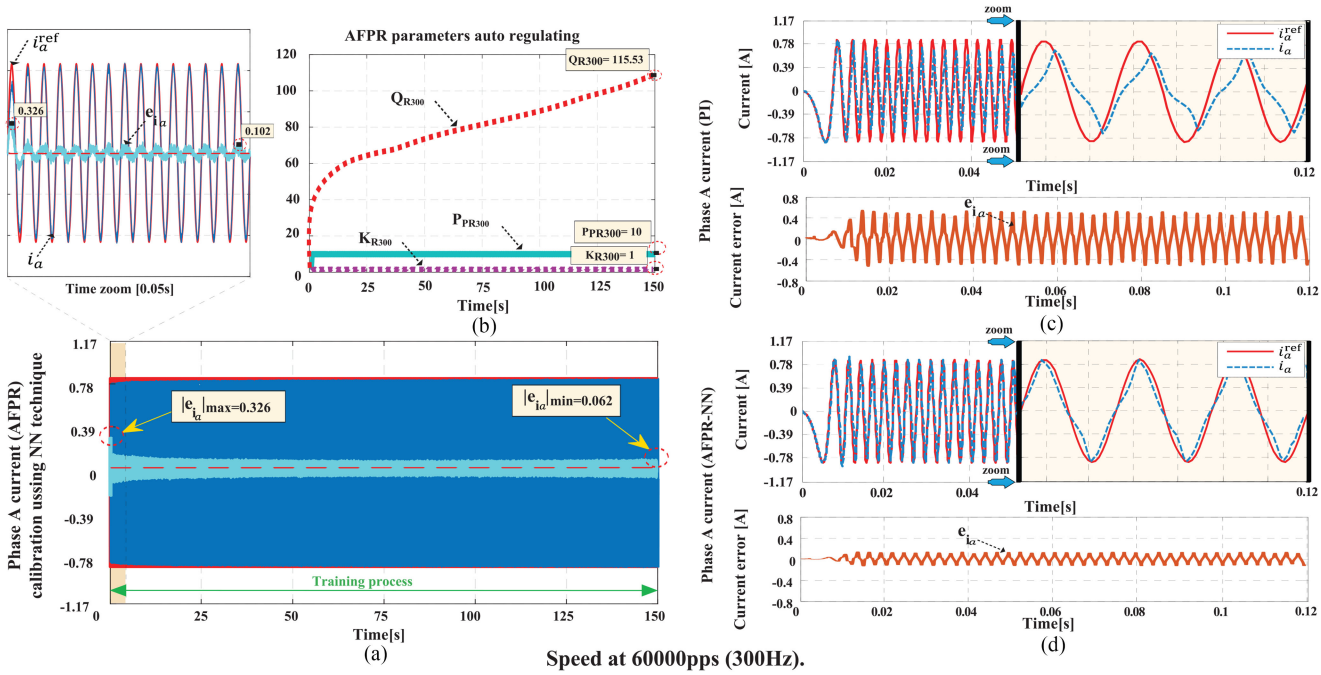

Fig. 16. NN calibration and current tracking performances of the conventional PI controller and the proposed AFPR-NN controller with $P_{\mathrm{PR}} \approx 10$, $K_R \approx 1$, $Q_R \approx 115.55$ at 300 Hz.

the position error, although the latter effect is not significant. The position tracking performance of the step motor under the conventional method and the proposed method is shown in Fig. 18. The results of three different speeds are: (a) 10 000 pps (50 Hz), (b) 30 000 pps (150 Hz), and (c) 60 000 pps (300 Hz). In these figures, the performance of the proposed method has the smallest position error. The steady-state compensation value α_{dc} made the SSPE approach zero, and the transient compensation value α_{ac} reduced the vibration of the motor. The effectiveness of the proposed method is shown most clearly in the target position. The target position II of the proposed method is of good stability and high accuracy when compared to the target position I of the conventional method. Specifically, the position errors of these methods are compared in Table II.

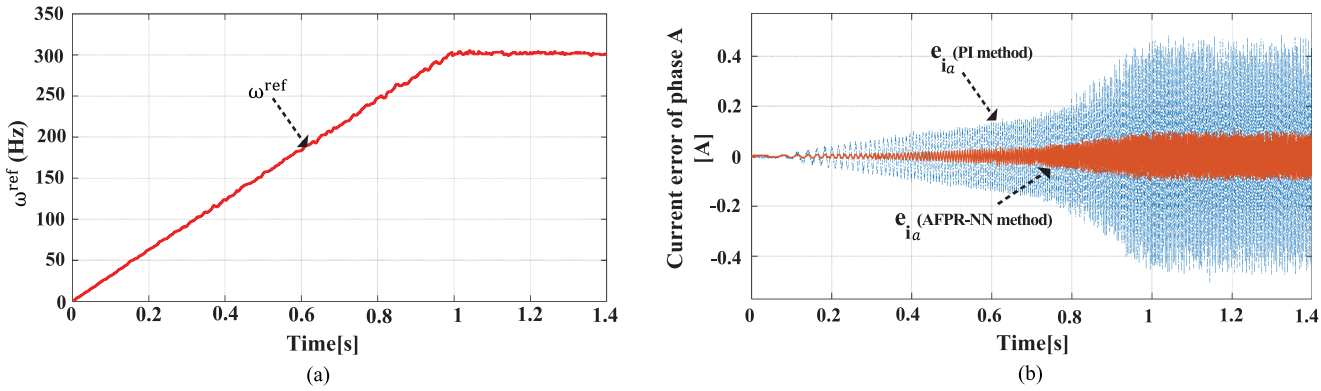

Fig. 17. Results of the sweep test. (a) Reference velocity of the stepper motor. (b) Current error of the PI and AFPR-NN method.

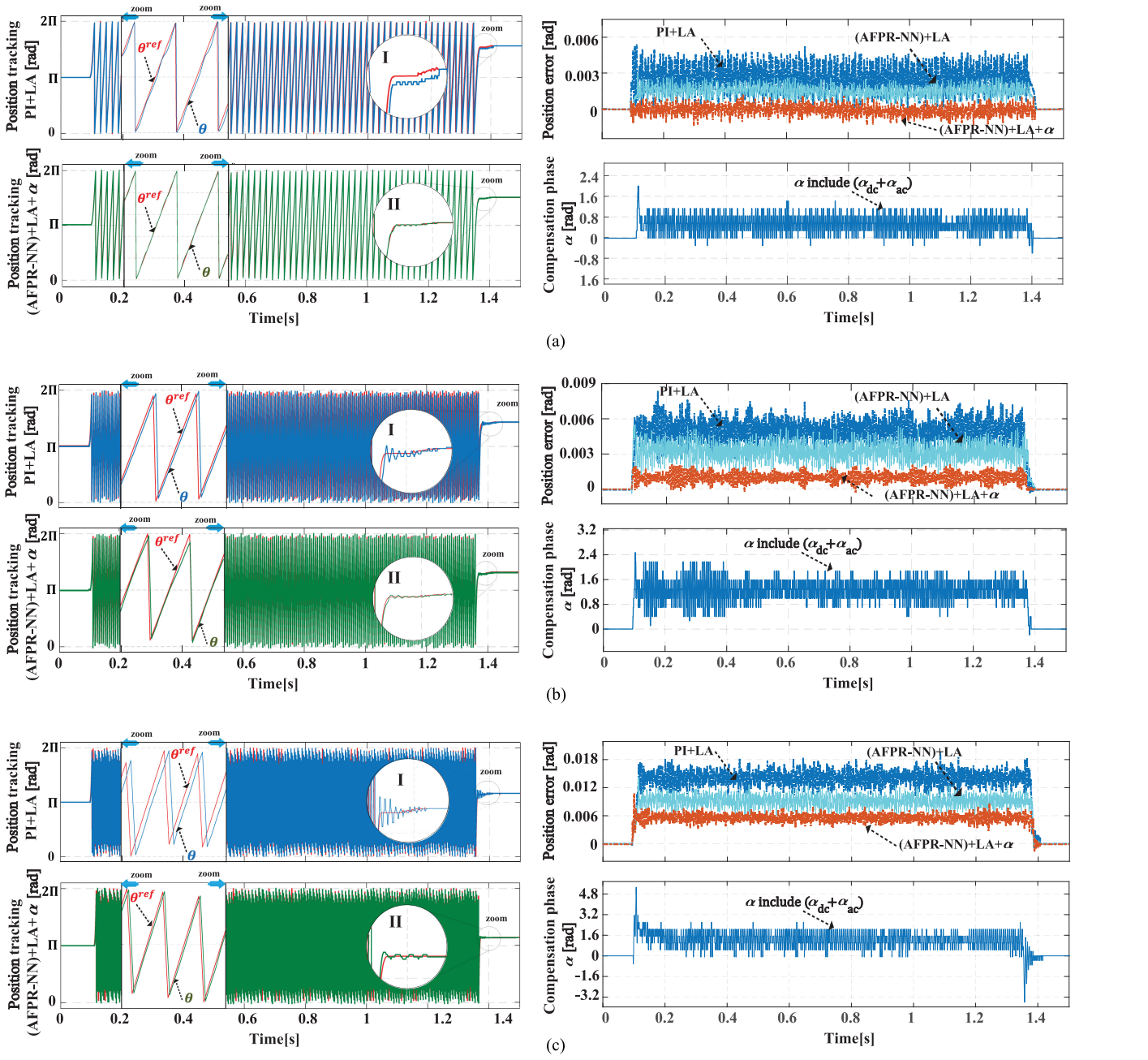

Fig. 18. Position tracking performance of the proposed methods compared with the conventional method (PI + LA) at low speed.

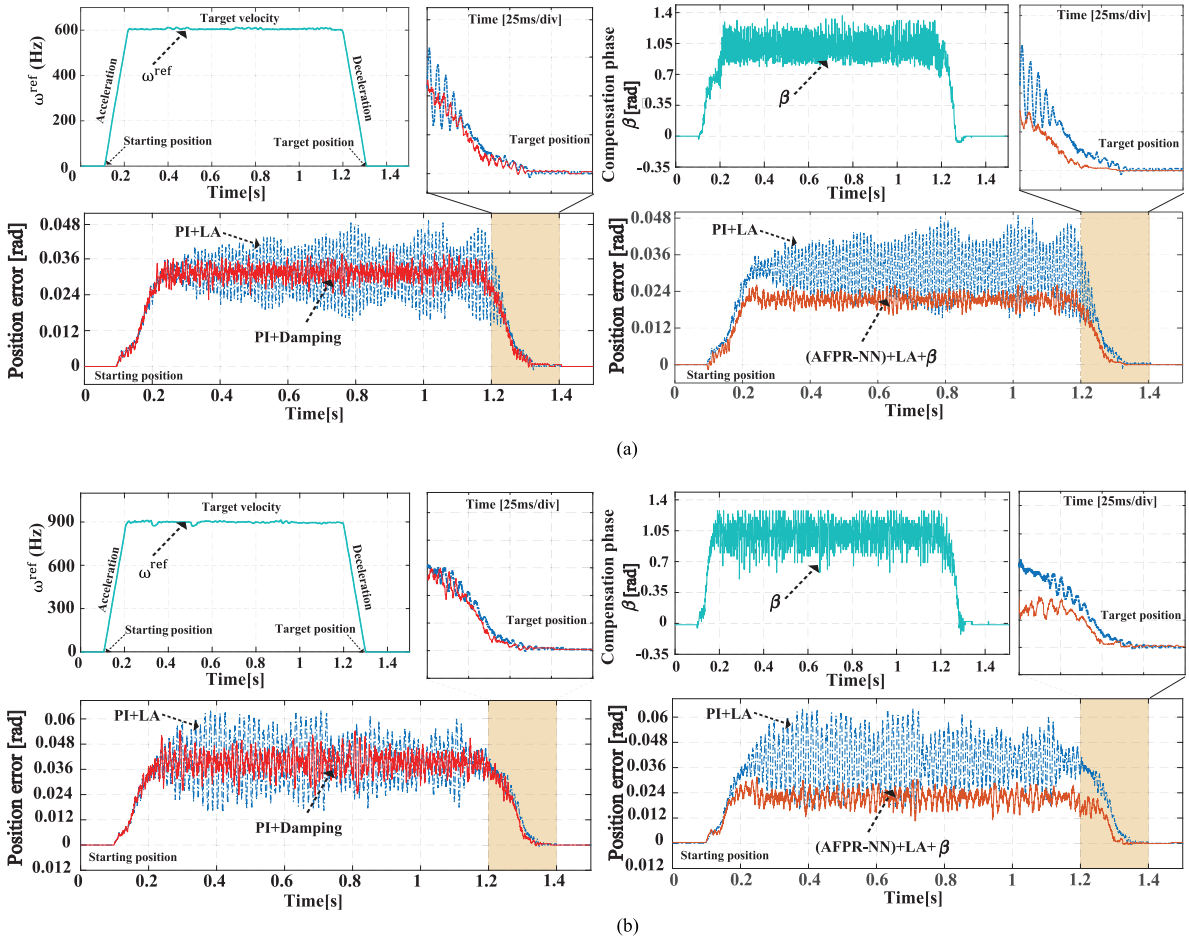

Fig. 19. Position tracking performance of the proposed method (AFPA − NN + LA + β) compared with the conventional method (PI + LA) and damping controller at high speed.

TABLE II
COMPARISON OF THE POSITION ERROR BETWEEN THE CONVENTIONAL METHOD WITH THE (AFPR-NN+LA) METHOD, AND WITH THE (AFPR-NN+LA+α) METHOD AT LOW SPEED

Speed [Hz]	PI+LA		AFPR-NN+LA		AFPR-NN+LA +α	
	Mean $\triangle\theta_{dc}$ [rad]	Max $\triangle\theta_{ac}$ [rad]	Mean $\triangle\theta_{dc}$ [rad]	Max $\triangle\theta_{ac}$ [rad]	Mean $\triangle\theta_{dc}$ [rad]	Max $\triangle\theta_{ac}$ [rad]
50Hz	0.0028	0.0051	0.0015	0.0032	0.0001	0.0011
150Hz	0.0057	0.0062	0.0031	0.0055	0.0014	0.0024
300Hz	0.0143	0.0092	0.0089	0.0075	0.0055	0.0048

TABLE III
COMPARISON OF THE POSITION ERROR BETWEEN THE CONVENTIONAL METHOD WITH AND DAMPING METHOD AND THE (AFPR-NN+LA+β) METHOD AT HIGH SPEED

Speed [Hz]	PI+LA		Damping		AFPR-NN+LA +β	
	Mean $\triangle\theta_{dc}$ [rad]	Max $\triangle\theta_{ac}$ [rad]	Mean $\triangle\theta_{dc}$ [rad]	Max $\triangle\theta_{ac}$ [rad]	Mean $\triangle\theta_{dc}$ [rad]	Max $\triangle\theta_{ac}$ [rad]
600Hz	0.032	0.0027	0.031	0.012	0.021	0.008
900Hz	0.038	0.0054	0.036	0.026	0.023	0.014

D. Experimental Results of a High-Speed Compensator

During high-speed operations, the oscillations of the error position are greater than at low speeds. Therefore, we designed a high-speed compensator to guarantee high-quality position control. The proposed method was compared to the damping method, which is described in the literature [22]. The damping method is given by

$$i_a^{\text{ref}} = I_{\max}\cos\left(\theta^{\text{ref}}\right) - \Delta I \sin\left(\theta^{\text{ref}}\right)$$
$$i_b^{\text{ref}} = I_{\max}\sin\left(\theta^{\text{ref}}\right) + \Delta I \cos\left(\theta^{\text{ref}}\right). \quad (43)$$

The experimental results at high speed are shown in Fig. 19(a) and (b). We can see both the damping method and proposed method, and we compared them with the conventional method, and with each other. The system was tested at a speed of 120 000 pps (600 Hz), and 180 000 pps (900 Hz). As shown, the conventional method without damping and the high-speed phase compensator vibrated very strongly. When we applied the damping method, the transient position error was reduced. However, the steady-state error was not removed. Therefore, we designed an advanced PID method with the parameters selected according to the standard stability (42), i.e., $K_p \approx 9.32$, $K_d \approx 0.06$, and

$K_i \approx 689.5$. The high-speed compensation value is also shown in Fig. 19(a) and (b) showing steady state and good accuracy at the target position. Table III compares the position errors and shows the favorable results of the reduced position error in the high-speed regions.

VI. Conclusion

We have developed a current controller with the proposed AFPR method using the NN calibration technique to guarantee the current tracking error of a stepper motor. The previous approaches to address this problem were based on conventional LA and damping techniques. However, these schemes resulted in a significant position error and a distortion in the position tracking performance. To compensate for the position error under low-speed operation, a new position tracking controller was proposed using our D&PC method with a low-speed compensator. In addition, the motor operates smoothly over the high-speed range. The position controller with a phase compensator was further enhanced with an adaptive PID controller to reduce the position error and distortion. All the proposed algorithms are simple and reliable and do not require any additional costs. To evaluate the effectiveness of the proposed controllers, we conducted experiments with different velocity profiles from low to high speeds. The experimental results were similar to the theoretical prediction, compensating for the phase lag of the current error, reducing the ripple, and decreasing the amplitude of the position error.

References

[1] Y. I. Son, I. H. Kim, D. S. Choi, and H. Shim, "Robust cascade control of electric motor drives using dual reduced-order PI observer," *IEEE Trans. Ind. Electron.*, vol. 62, no. 6, pp. 3672–3682, Jun. 2015.

[2] J. W. Jung, Y. S. Choi, V. Q. Leu, and H. H. Choi, "Fuzzy PI-type current controllers for permanent magnet synchronous motors," *IET Electr. Power Appl.*, vol. 5, no. 1, pp. 143–152, Jan. 2011.

[3] M. Marufuzzaman, M. B. I. Reaz, and M. A. M. Ali, "FPGA implementation of an intelligent current dq PI controller for FOC PMSM drive," in *Proc. Int. Conf. Comput. Appl. Ind. Electron.*, 2010, pp. 602–605.

[4] W. Kim, D. Shin, and C. C. Chung, "Microstepping using a disturbance observer and a variable structure controller for permanent magnet stepper motors," *IEEE Trans. Ind. Electron.*, vol. 60, no. 7, pp. 2689–2699, Jul. 2013.

[5] H. Komurcugil, N. Altin, S. Ozdemir, and I. Sefa, "Lyapunov-function and proportional-resonant-based control strategy for single-phase grid-connected VSI with LCL filter," *IEEE Trans. Ind. Electron.*, vol. 63, no. 5, pp. 2838–2849, May 2016.

[6] A. Rubaai, M. J. Castro-Sitiriche, M. Garuba, and L. Burge, "Implementation of artificial neural network-based tracking controller for high-performance stepper motor drives," *IEEE Trans. Ind. Electron.*, vol. 54, no. 1, pp. 218–227, Feb. 2007.

[7] D. Shin, W. Kim, Y. Lee, and C. C. Chung, "Phase-compensated microstepping for permanent-magnet stepper motors," *IEEE Trans. Ind. Electron.*, vol. 60, no. 12, pp. 5773–5780, Dec. 2013.

[8] G. Wang, R. Yang, and D. Xu, "DSP-based control of sensorless IPMSM drives for wide-speed-range operation," *IEEE Trans. Ind. Electron.*, vol. 60, no. 2, pp. 720–727, Feb. 2013.

[9] M. Bodson, J. N. Chiasson, R. T. Novotnak, and R. B. Rekowski, "High performance nonlinear feedback control of a permanent magnet stepper motor," *IEEE Trans. Control Syst. Technol.*, vol. 1, no. 1, pp. 5–14, Mar. 1993.

[10] M. Defoort, F. Nollet, T. Floquet, and W. Perruquetti, "A third-order sliding-mode controller for a stepper motor," *IEEE Trans. Ind. Electron.*, vol. 56, no. 9, pp. 3337–3346, Sep. 2009.

[11] W. Kim, D. Shin, and C. C. Chung, "Microstepping with nonlinear torque modulation for position tracking control in permanent magnet stepper motors," *IEEE Trans. Control Syst. Technol.*, vol. 21, no. 5, pp. 1971–1979, Sep. 2013.

[12] T. S. Hwang, J. K. Seok, and D. H. Kim, "Active damping control of linear hybrid stepping motor for cogging force compensation," *IEEE Trans. Magn.*, vol. 42, no. 2, pp. 329–334, Feb. 2006.

[13] K. W. Tsui, N. C. Cheung, and K. C. Yuen, "Novel modeling and damping technique for hybrid stepper motor," *IEEE Trans. Ind. Electron.*, vol. 56, no. 1, pp. 202–211, Jan. 2009.

[14] J. Chiasson, *Modeling and High-Performance Control of Electric Machines.* Hoboken, NJ, USA: Wiley-Interscience, 2005.

[15] Q. N. Le and J. W. Jeon, "An open-loop stepper motor driver based on FPGA," in *Proc. Int. Conf. Control, Automat. Syst.*, Oct. 2007, pp. 1322–1326.

[16] R. Teodorescu, F. Blaabjerg, M. Liserre, and P. Loh, "Proportional resonant controllers and filters for grid-connected voltage-source converters," *Proc. Inst. Elect. Eng.-Elect. Power Appl.*, vol. 153, no. 5, pp. 750–762, Sep. 2006.

[17] W. Lenwari, "Reivew of a high performance control of AC signals based on a proportional plus resonant compensator," *Suranaree J. Sci. Technol.*, vol. 15, no. 4 pp. 334–344, Oct. 2008.

[18] M. T. Hagan, H. B. Demuth, M. H. Beale, and O. D. Jess, *Neural Network Design*, 2nd ed. Boston, MA, USA: Martin Hagan, 2014.

[19] A. Takemori, Y. Kuwano, Y. Takahashi, and H. Taka, "Stepping motor driver," U.S. Patent 6 850 026, Feb. 1, 2005.

[20] S. A. Schweid, J. E. McInroy, and R. M. Lofthus, "Closed loop low-velocity regulation of hybrid stepping motors amidst torque disturbances," *IEEE Trans. Ind. Electron.*, vol. 42, no. 3, pp. 316–324, Jun. 1995.

[21] M. Bodson, J. S. Sato, and S. R. Silver, "Spontaneous speed reversals in stepper motors," *IEEE Trans. Control Syst. Technol.*, vol. 14, no. 2, pp. 369–373, Mar. 2006.

[22] K. M. Le, H. V. Hoang, and J. W. Jeon, "An advanced closed-loop control to improve the performance of hybrid stepper motors," *IEEE Trans. Power Electron.*, vol. 32, no. 9, pp. 7244–7255, Sep. 2017.

Hoang Ngoc Tran received the B.S degree in mechatronics engineering from the Ho Chi Minh City University of Technology, Ho Chi Minh City, Vietnam, in 2015. He is currently working toward the Ph.D. degree in electrical and computer at the School of Information and Communication Engineering, Sungkyunkwan University, Suwon, South Korea.

His research interests include signal processing, motion control, robotics, and embedded systems.

Kien Minh Le received the B.S. degree in electrical engineering from the Hanoi University of Technology, Hanoi, Vietnam, in 2006, the M.S. degree in automation from Le Quy Don Technical University, Hanoi, in 2011, and the Ph.D. degree in electrical and computer engineering from Sungkyunkwan University, Suwon, South Korea, in 2017.

He is currently a Postdoctoral Researcher with the School of Information and Communication Engineering, Sungkyunkwan University, South Korea. His research interests include motion control and embedded systems.

Jae Wook Jeon (S'82–M'84) received the B.S. and M.S. degrees in electronics engineering from Seoul National University, Seoul, South Korea, in 1984 and 1986, respectively, and the Ph.D. degree in electrical engineering from Purdue University, West Lafayette, IN, USA, in 1990.

From 1990 to 1994, he was a Senior Researcher with Samsung Electronics, Suwon, South Korea. In 1994, he was an Assistant Professor with the School of Information and Computer Engineering, Sungkyunkwan University, Suwon, where he is currently a Professor. His research interests include robotics, embedded systems, and factory automation.